ILASS–Europe 2017, 28th Conference on Liquid Atomization and Spray Systems, 6-8 September 2017, Valencia, Spain
http://dx.doi.org/10.4995/ILASS2017.2017.4652

Development of an evaporation model for the dense spray region in Eulerian-Eulerian multiphase flow simulations

Stefano Puggelli*[,1], Lorenzo Palanti [1], Antonio Andreini [1], François-Xavier Demoulin[2]
[1] Department of Industrial Engineering (DIEF), University of Florence, Italy
[2] CNRS CORIA UMR 6614, University of Rouen, France
*Corresponding author: stefano.puggelli@htc.de.unifi.it

Abstract
In the present study, a novel implicit numerical model to describe evaporation phenomena in the dense spray region is proposed. The main aim is to go beyond the limits of standard vaporization models, which are normally based on a dilute spray assumption, to deal with high liquid volume fractions. The proposed method is based on an a priori computation of steady state equilibrium conditions reached by a system composed by liquid, vapour and air at constant pressure combined with a modelled characteristic time of evaporation. Such equilibrium composition and temperature is then used inside numerical calculations to compute evaporation source terms. The new formulation allows to simulate evaporation process in the dense zone of the spray, where, due to the extremely low thermal relaxation time, classical explicit method can lead to unphysical results. Such innovative approach has been implemented in a multiphase solver in the framework of the CFD suite OpenFOAM. An Eulerian-Eulerian solver, derived from the Eulerian Lagrangian Spray Atomization (ELSA) model, has been used, in order to correctly describe the liquid-gas flow without assumptions on the topology of the liquid phase. Evaporation source terms have been modelled as function of the amount of surface available for mass and heat transfer. An analysis of the solver has been carried out in RANS framework in order to highlight the capabilities of the approach in dealing with high liquid volume fraction regions with a physically consistent representation of evaporation phenomena.

Keywords
Spray modelling, ELSA, Eulerian-Eulerian methods, Evaporation modelling.

Introduction

The future standards on pollutants emissions expected by ICAO-CAEP [1] for the next generation of civil aero-engines have pushed the attention towards the introduction of lean burn technology in aeronautical framework. Here, a drastic reduction of NOx levels can be achieved working on a narrow range of temperature and equivalence ratio. Therefore, all the issues related to liquid fuel atomization and air-fuel mixing have to be carefully investigated and Computational Fluid Dynamics (CFD) has been gaining strong attention for the design process.
In this framework, the numerical method chosen for the modelling of the liquid phase can have a strong impact on both simulation accuracy and computational effort. Standard Eulerian-Lagrangian (E-L) approaches, which are based on tracking single liquid discrete entities (i.e. parcels), are characterized by a straightforward introduction of the main interactions between the gas and the liquid phase, even if they are not theoretically suitable in the near injection region where the spray is really dense. An extensive use of experimental correlations in order to introduce the effects of primary breakup inside numerical calculations is therefore required. However, this strategy is not general since a strong spreading between the huge number of available experimental correlations can be determined for the same configuration and operating conditions.
Besides, Eulerian-Eulerian (E-E) methods are very attractive since several ways, associated to different computational costs, can be here used to solve the kinetic Boltzmann-Williams equation [2]. This has determined a copious research on Eulerian methods starting from approaches based on a discretization of the spray distribution along the diameter space (i.e. sectional approaches [3]) to other built on the calculation of some moments of the spray probability density function (such as Quadrature Method Of Moments [4] or Direct Quadrature Method Of Moments [5]. Other approaches, such as entropy maximization [6] or moments with interpolative closure [7], can be also found in the literature but their description goes beyond the scope of the present work. Recent contributions in this area have shown the suitability of these methods in describing the most important features of liquid sprays [8]. Nevertheless, since all these approaches are theoretically based on the Boltzmann-Williams equation, they can be used only when the spray is composed by individual droplets with well-defined features as position or diameter. Therefore, in order to consider also the dense zone, diffuse interface models have been considered in the present work. In these models, the interface is considered as a mixing zone where both liquid and gas phases coexist at the same macroscopic position with an occupied portion of volume defined by the liquid volume fraction (α_l). In this context, several family of models have been developed in technical literature and in the present analysis the Eulerian-Lagrangian Spray Atomization (ELSA) model has been considered [9, 10]. In ELSA framework, an Eulerian mixture model is employed to describe the near-nozzle dense spray region, whereas a lagrangian population is initialized when the spray becomes dilute. Therefore, a full atomization process from pure liquid to dispersed droplets can be considered. Such approach has been already validated on different spray configurations [9, 10] and its capabilities extended to consider the strong interactions between liquid and gas phase that characterize aero-engine applications [11].

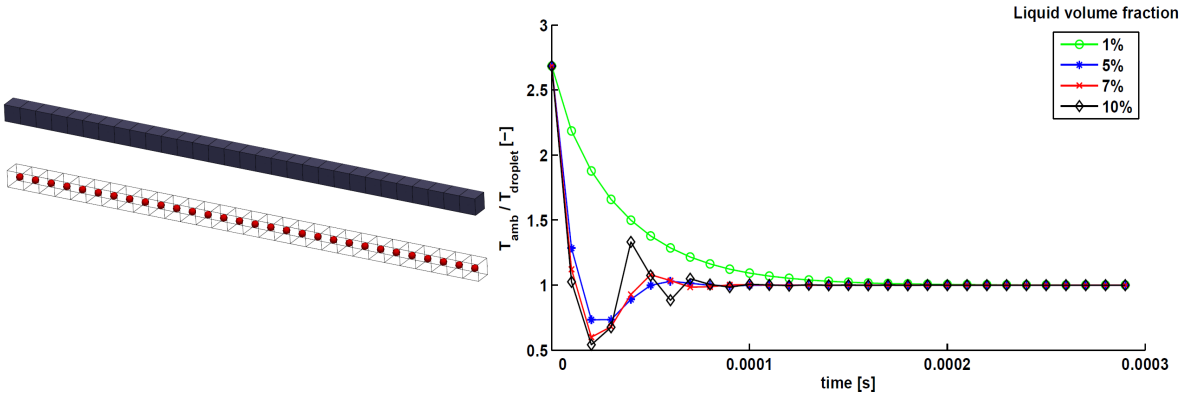

Figure 1. Ratio of ambient and droplet temperature with the respect of time for several liquid volume fraction using an explicit formulation for evaporation modelling.

However, large part of such contributions have been performed in iso-thermal test conditions or using modelling strategies for the evaporation process directly derived from a lagrangian context. For instance, in [9] evaporation effects in the dense zone are neglected, whereas in [12] an explicit formulation is employed for the Eulerian region of ELSA and the vaporization rate is calculated from the local temperature considering the fuel vapour as saturated on the liquid surface. However, such explicit formulation can lead to strong temperature undershootings on the gas side in regions where α_l is really high (i.e. near injector regions). Considering for instance the 1-D test case shown in Figure 1 where a cloud of droplets (highlighted in red) is introduced inside a hot stagnant environment, it is possible to calculate the ratio between the gas phase and liquid temperature with respect to time for several values of cell liquid volume fraction. The source/sink terms due to evaporation are here implemented through an explicit formulation and in particular the sink term employed for the gas phase energy equation can be written as:

$$\frac{dh}{dt} = HA_{drop}(T_l - T_g) - \frac{dm}{dt}L \tag{1}$$

where h stands for gas phase enthalpy, dh/dt for its own variation in time, H and A_{drop} for heat transfer coefficient and droplet surface area respectively. Liquid temperature and gas phase temperature are mentioned as T_l and T_g while dm/dt and L are evaporation rate and latent heat of vaporization. It should be pointed out that increasing the liquid volume fraction, this explicit formulation can possibly lead to unbounded values of gas phase temperature. In fact, as soon as dm/dt has been estimated and temperatures have been fixed, depending on dt a certain value of dh can be computed. If dt it is not sufficiently short, dh may be large enough to determine a sharp decrease of gas phase temperature. Then, dealing with a very small gas phase fraction it is possible to obtain temperature undershoots as reported on the right side of Figure 1. Clearly, such issue can be overcome by reducing the simulation time step but with a strong increase of the computational cost considering that as the liquid volume fraction tends to 1.0 the time step should go to zero in order to avoid such instabilities.
Therefore, an implicit formulation can be used to robustly include evaporation inside numerical methods and to avoid this unphysical behaviour in the dense spray region. Implicit approaches are based on a priori calculation of a local equilibrium state established between the volume of liquid and gas that coexist in the same control volume. Such thermodynamic equilibrium condition is then used to compute the evaporation rate as will be explained in detail in the next section. Such implicit approaches are normally based on the assumption that locally the liquid is completely evaporated at equilibrium state [13]. This is not generally true, since for non diluted cases some amount of liquid remains even at equilibrium state. This is the case of the near injector region where the liquid core may be slightly affected by evaporation, but can heavily determine the overall atomization. In [14, 15] an original implementation of evaporation modelling based on local adiabatic saturation conditions is shown, but it is assumed that the characteristic time scale of vaporization is the calculation time step (dτ). It is essentially based on the hypothesis that the vaporization is so quick that it is completed within the simulation time-step. However, this is not generally true since the particle relaxation time can vary inside the domain based on the local flow-field. For instance in [16], a security factor is introduced between the simulation and particle time step in order to correctly catch the dynamic and thermal evolution of the liquid phase.
To overcome such limitations and to extend the ELSA capabilities in dealing with evaporation in the dense spray region with a more physical characteristic time scale, a novel implicit evaporation modelling strategy has been developed in the framework of the open source code OpenFOAM. Considering that the attention here is mainly focused on the dense zone, only the Eulerian-Eulerian solver derived from ELSA has been considered for the present study. The next section is therefore devoted to the description of such E-E solver and to the characterization of the modelling strategy employed to include evaporation. In the second part of the paper, the available experimental data from the Engine Combustion Network (ECN) database for a diesel jet in evaporating test conditions are used to assess the proposed model on a realistic configuration.

Numerical methods

Compressible ELSA model

In the E-E model derived from ELSA model, the two phase flow is analysed as a single phase flow composed of two species with highly variable density. Therefore, beyond the equation for the mixture momentum (U), the solver essentially consists of an equation for the liquid volume fraction to predict the liquid evolution and of an equation for liquid/gas interface per unit of volume (Σ) to model the breakup process and to consider a polydisperse spray distribution. Locally the spray Sauter Mean Diameter (SMD) can be directly calculated from α_l and Σ as $SMD = 6\alpha_l/\Sigma$. The reader interested in a detailed description of the ELSA formalism and its possible extensions to include the effects of a slip velocity between liquid and gas (i.e. Quasi Multiphase Eulerian approach) is addressed to the specific literature [9, 10, 11].

Starting from such E-E approach, a fully compressible solver has been firstly developed for evaporative test condition. In fact, the energy transfer from gas to liquid plays a key role and, due to the high temperature variation, the density of the gas phase can not be clearly considered constant. A transport equation for vapour volume fraction has been first of all introduced alongside the one for α_l. Both of them are now solved in a compressible fashion and source terms due to evaporation have been added. The equation are written in RANS context, thus all variables are considered as mean Reynolds variables. A standard gradient closure is applied for turbulent fluxes but it is not here discussed for the sake of brevity and only the vaporisation term is explained in detail.

$$\frac{\partial \rho_l \alpha_l}{\partial t} + \frac{\partial \rho_l \alpha_l U_i}{\partial x_i} - \frac{\partial}{\partial x_i}\left[\left(\rho_l D_l + \frac{\mu_t}{Sc_{tl}}\right)\frac{\partial \alpha_l}{\partial x_i}\right] = -\dot{\alpha}_{ev} \tag{2}$$

$$\frac{\partial \rho_v \alpha_v}{\partial t} + \frac{\partial \rho_v \alpha_v U_i}{\partial x_i} - \frac{\partial}{\partial x_i}\left[\left(\rho_v D_v + \frac{\mu_t}{Sc_{tv}}\right)\frac{\partial \alpha_v}{\partial x_i}\right] = \dot{\alpha}_{ev} \tag{3}$$

where ρ and D represents the bulk density and diffusivity for liquid and vapour, Sc_t is the turbulent Schmidt number, μ_t is the turbulent viscosity and $\dot{\alpha}_{ev}$ is the contribution of evaporation. The subscripts l and v stand for liquid and vapour respectively. Clearly, the air volume fraction is directly calculated from $\alpha_l + \alpha_v + \alpha_a = 1$, where the subscript a refers to air.

Two energy equations, one for liquid and one for gas phase, written in terms of temperatures have been also introduced and the contribution of evaporation appears as additional source term ($\dot{T_{ev}}$). Below, the energy equation for the liquid phase is shown.

$$\frac{\partial \rho_l \alpha_l c_{p_l} T_l}{\partial t} + \frac{\partial \rho_l \alpha_l c_{p_l} T_l U_i}{\partial x_i} - \frac{\partial}{\partial x_i}\left(\alpha_l \frac{\mu_t}{Pr_{tl}}\frac{\partial T_l}{\partial x_i}\right) = \dot{T_{ev}} \tag{4}$$

where c_p is the specific heat and Pr_t is the turbulent Prandtl number. A sink term due to evaporation should be introduced also for the Σ equation, but it has been neglected in the present study since it should have a minor impact in the dense region that is dominated by the breakup process because of the high value of the Weber number. In the further diluted part, a model similar to the one used in [9] may be applied.

Clearly, special attention has been devoted to the dynamic expression of the evaporation source terms in the previous system of equations, exploiting the following implicit formulation:

$$\dot{\alpha}_{ev} = \rho_l \left(\frac{\alpha_{l_{eq}} - \alpha_l}{\tau_m}\right) \tag{5}$$

$$\dot{T}_{ev} = \rho_l \alpha_l cp_l \left(\frac{T_{l_{eq}} - T_l}{\tau_T}\right) \tag{6}$$

where $\alpha_{l_{eq}}$ and $T_{l_{eq}}$ represent the equilibrium state that locally the liquid/gas system reaches in terms of remaining liquid volume and temperature with two rates defined by τ_m and τ_T. Similar formulations are employed also for the gas phase and they have not been reported here for the sake of brevity. Equations 5 and 6 lead to an unconditionally stable system on a mathematical point of view, even if a proper calculation of equilibrium state and evaporation rates has to be provided and it will be detailed in the next sub-section.

Equilibrium calculation and evaporation rates

Firstly, it is important to recall that two phases of a pure substance are in an equilibrium state when both phases share the same value of the specific Gibbs function. Mass transfer plays a key role in equilibrium composition for a vaporizing system and it is of primary importance in calculating the equilibrium temperature since if some liquid evaporates (or some vapour condensates) a variation in total enthalpy occurs due to the latent heat of vaporization. Therefore, considering the evaporation process in a two-phase, two-component system inside an isolated volume at constant pressure, where mass transfer takes place from liquid to vapour phase, it is theoretically possible to calculate the equilibrium temperature of the system as:

$$T_{eq} = \frac{m_a c_{p_a} T_g + m_l c_{p_l} T_l + m_v c_{p_v} T_g - (m_{v_{eq}} - m_v) L}{m_a c_{p_a} + m_{l_{eq}} c_{p_l} + m_{v_{eq}} c_{p_v}} \tag{7}$$

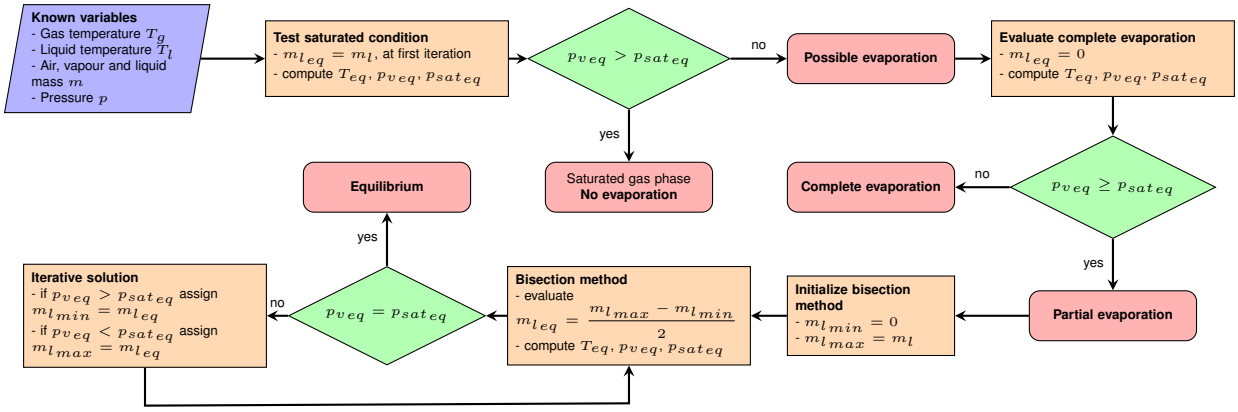

Figure 2. Method implemented for computation of equilibrium composition and temperature

Another relationship is now necessary to estimate the composition at equilibrium. In the present study, it has been chosen to directly calculate the mass of liquid at equilibrium ($m_{l_{eq}}$) and consequently the vapour mass as $m_{v_{eq}} = m_v - (m_{l_{eq}} - m_l)$, where m_l and m_v are the local mass of liquid and vapour at time t. In addition, it has been considered that phase equilibrium for a two phase system can be defined also when the vapour pressure in the air is equal to the saturation pressure of liquid at the liquid temperature. It means that:

$$p_v = p_{sat}(T_{eq}) \tag{8}$$

where partial vapour pressure (p_v) can be easily calculated through the number of moles of air and vapour in the fraction of volume available for the gas phase. Therefore, using Equations 7 and 8, an iterative cycle can be set to determine the equilibrium state varying $m_{v_{eq}}$ until Equation 8 is satisfied. The loop is briefly summarized in Figure 2. At the beginning, the saturated condition is evaluated by placing $m_{l_{eq}} = m_l$. T_{eq} is therefore calculated by equation 7, $p_{v_{eq}}$ by equation 8 and $p_{sat_{eq}}$ by the standard Antoine equation using T_{eq}. If the obtained vapour partial pressure is higher than the saturation pressure, no evaporation will be allowed since the gas phase is already saturated by vapour. In this case, only an heat transfer is introduced between phases and a proper T_{eq} is calculated.
On the contrary, if some evaporation is possible, the case of complete evaporation is evaluated and two possible situations are therefore considered:

1. if $p_{v_{eq}} < p_{sat_{eq}}$, the whole liquid will be evaporated and the final equilibrium temperature for the liquid is set equal to the wet bulb value, whereas the one for the gas is computed thanks to Equation 7.

2. if $p_{v_{eq}} \geq p_{sat_{eq}}$, only partial evaporation will take place. This situation leads to an iterative cycle based on Equation 8 and in the present study a simple bisection method has been employed because of his stability and boundedness. Further developments are surely required on this point to decrease the overall computational effort.

Finally, the obtained $m_{l_{eq}}$ and T_{eq} are used to compute source terms for transport equation through Equations 5 and 6.
The remaining parameters that needs now to be defined are τ_m and τ_T. There is not modelling proposal for the rate of vaporisation to be applied for any liquid volume fraction yet. To overcome this difficulty a first proposal is based on the Abramzon-Sirignano model [17]. The advantage is to recover on more diluted part the correct vaporisation rate, but the characteristic vaporisation time scale is underestimated in the dense part. However, it is worth mentioning that this error should be partially compensated by the implicit method. In fact, the equilibrium value $m_{l_{eq}}$ should be correctly computed through the equilibrium cycle and the modelling approximation is only given by the τ computation. In addition to that, in the dense zones, where α_l approaches to one, the volume left for gas phase is generally small and it will be rapidly cooled and saturated by vapour. Therefore, the mass of liquid allowed to evaporate will be small as well as the characteristic τ. This suggests that the time required by the system to achieve the equilibrium is not so relevant and far more attention must be paid to the estimation of the correct equilibrium state at least for the near injector region. Further developments are required on this point, introducing an increasing number of geometrical properties of the liquid/gas interface: a model for the curvature of the liquid surface is now under investigation to this end. However, using previous assumption, it is possible to obtain the expressions of τ_m and τ_T shown below:

$$\tau_m = \frac{m_l - m_{l_{eq}}}{\dot{m}} = \frac{m_l - m_{l_{eq}}}{\pi d n_d Sh^* D_g \rho_g \ln(1 + B_M)} \tag{9}$$

$$\tau_T = \frac{T_{l_{eq}} - T_l}{\frac{\dot{Q} - \dot{m}L}{c_{p_l} m_l}} \tag{10}$$

Table 1. Operating conditions of the ECN test cases under investigation.

	Test case 1	Test case 2	Units
Orifice nominal diameter	0.084	0.084	mm
Mean injection pressure	150	50	MPa
Mean injection velocity	$\sim$ 600	$\sim$ 300	m/s
Fuel density	713	713	kg/m^3
Fuel temperature	363	363	K
Ambient temperature	900	900	K
Ambient pressure	6.05	6.05	MPa
Area contraction coefficient	0.98	0.98	-

where d and n_d can be directly calculated from α_l and Σ as shown below:

$$d = \frac{6\alpha_l}{\Sigma} \tag{11}$$

$$n_d = \frac{V_{liquid}}{V_{droplet}} = \frac{V_{liquid}}{V_{cell}} \frac{V_{cell}}{V_{droplet}} = \alpha_l \frac{6}{\pi d^3} V_{cell} \tag{12}$$

Moreover, in Equation 10, $\dot{Q}$, which is the heat transfer between phases, appears and it can be calculated as:

$$\dot{Q} = \pi d n_d N u^* k_g \frac{\ln\left(1 + B_T{}'\right)}{B_T{}'} (T_g - T_l) \tag{13}$$

where k_g is the gas thermal conductivity, Nu^* is the corrected Nusselt number to account for the effects of Stefan flow and $B_T{}'$ is the thermal Spalding number. Due to the lack of slip velocity between phases, Reynolds number employed in the definition of Nu^* and Sh^* is calculated using the fluctuating component of velocity [18]. Such approximation will be avoided employing QME [11] in a future implementation of the solver. For the sake of brevity, the complete expression of these terms is not here detailed but it is possible to recast a formulation of each one in terms of the characteristics variables of ELSA (i.e. α_l and Σ). It should be pointed out that all these quantities are valid both for the dilute and dense spray region since they are based only on geometrical properties of the droplet-gas interface, which are defined in all the domain.

Validation of ELSA under evaporating test conditions

Description of the test case

The experimental test case investigated in the present work has been studied at Sandia National Laboratories and it is composed by a common rail injection system, used to supply fuel to a solenoid-actuated diesel injector [19]. The nominal diameter of the injector here analysed is 0.084 mm and the experimental apparatus is described in detail in [19].

Several experimental data are available and, for the evaporating non-reacting test conditions here studied, the specific rail pressure ranges from 50 to 150 MPa and the spray is injected into an ambient density of 22.8 kg/m^3, corresponding to an ambient pressure of approximately 6 MPa at 900 K. A single component n-dodecane fuel is used to allow a complete knowledge of the physical and chemical properties. The injected fuel, thanks to the injection velocity and to the high temperature of the combustion chamber, rapidly breakups and evaporates, even if no combustion happens, because of the non-reactive environment. Injection duration is different for the various measurements, but it always overcome 4 ms in order to achieve the quasi-steady period of spray development.

Liquid length is measured through high-speed Mie scatter images using a 3% threshold of maximum intensity. For steady liquid penetration the period between 0.5 and 1.4 ms is considered [19]. Furthermore, Rayleigh scatter imaging is used to obtain several contour data for vapour fraction in order to determine both its axial and radial distributions. Data for vapour are available starting from 17.85 mm after the injection point until 50 mm downstream. In Table I the main operating conditions of the analysed test cases are summarized.

It should be pointed out that in terms of evaporation modelling the test case is really challenging since a large region where α_l tends to 1.0 can be found. On a theoretical point of view, this would constrain E-E solvers based on an explicit strategy to strongly reduce the time step size to avoid an unphysical behaviour of the vaporization source terms. Such issue should not appear using the modelling strategy here proposed, since the employment of an implicit formulation leads to a stable treatment of vaporization and to a time step definition just related to the local Courant-Friedrichs-Lewy (CFL) condition, determined by the flow-field velocity and mesh size.

Numerical setup

Calculations here reported have been realized using OpenFOAM v. 3.0.1. Simulations have been carried out on the axi-symmetric computational domain shown in Figure 3 where a zoom of the mesh in the near injection region is also shown. The domain is a 5 degrees sector of the whole domain with 1 element in the azimuthal direction. The axial and radial extensions of such domain are smaller than the experimental chamber (i.e. 108mm x 108mm

in experiments against 100mm x 20mm in present calculations), but it has been shown [15, 20] that it should not impact the jet evolution and the atomization process. Furthermore, considering that the focus of the present work is on evaporation modelling, the injector duct has not been included and the diameter has been reduced based on the area contraction coefficient experimentally measured (see Table I).

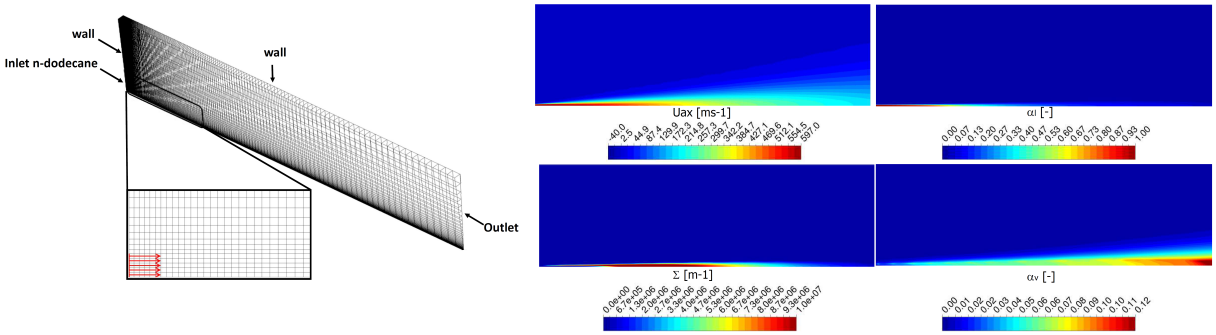

Figure 3. Computational domain (left) and evolution of ELSA variables for Test case 1 (right).

Such assumption allows us to neglect the cavitation inside the nozzle that would affect the real velocity profile and to concentrate the study just on the downstream region. As shown in [15, 20], where ELSA formulation is used to model the liquid/gas interface for the same test case, a mesh sizing with 10 elements along the injector diameter is able to properly reproduce the main features of the flow-field together with the liquid-air mixing. As suggested in [20], the aspect ratio of the cells comprised in the inlet patch is kept close to 1.0, while they are stretched in radial and axial direction. Therefore, a structured mesh counting 12500 cells with a size of 0.008 mm at the injector exit was generated.
Mass flow rate is imposed at the injector inlet following the available experimental data, whereas a static pressure is prescribed at the outlet. All the walls are treated as smooth, non-slip and adiabatic, whereas cyclic conditions have been applied on the two lateral patches.
The used time step has been chosen in order to ensure a control of the Courant number lower than one inside the computational domain. Therefore, all calculations were performed with dτ=1.5e-8 s for Test case 1 considering the high velocity of the liquid jet, whereas it has been increased to dτ=2.5e-8 s for Test case 2.
With regard to turbulence modelling, a standard κ-ϵ model has been employed. Following results shown in [15], a sensitivity study on the value of the characteristic constant $C_{\epsilon 1}$, in order to better predict the evolution of the jet, has been also performed. The investigated values are 1.44, 1.52 and 1.60 but for the sake of brevity, such analysis is not reported here. In fact, it has been pointed out that standard values of κ-ϵ constants (i.e. $C_{\epsilon 1}$=1.44) are able to reproduce vapour jet spreading with an overall good agreement, while the modified ones are not able to catch the lateral turbulent dispersion of the vapour.
The solver follows a classical segregated PISO method to solve the pressure-velocity coupling. Both convective and diffusive fluxes have been discretized following second order schemes whereas first order Euler scheme has been employed for time advancement.

Results

Figure 3 shows velocity and liquid-gas interface density evolutions together with liquid and vapour fraction contours obtained with ELSA on Test case 1 on a window of 10 mm x 3 mm after the injector exit. The liquid jet, due to its high Weber and Reynolds numbers, enters the chamber and undergoes a quick atomization process, which is pointed out by the zone where the production of Σ is really high. Such violent atomization is related to the growth of instabilities on the liquid surface due to the turbulent interactions with the gas phase, but it is also strongly affected by the heat-up and evaporation of liquid that take place immediately in the near injection region. A liquid core is therefore generated and the spray tends progressively to evaporate producing a region with a non-negligible volume of n-dodecane vapour. It should be pointed out that at the end of the selected window, the vapour volume fraction exceeds already the 10% and this can have an important effect in the stabilization mechanism if reacting test conditions are considered. Furthermore, even in regions where the liquid volume fraction is really high (i.e. $\alpha_l \simeq$ 0.8-0.9) the code is able to robustly determine a non zero evaporation rate with a consequent production of fuel vapour. In these regions it is likely that an explicit method shows strong numerical instabilities and undershootings in gas phase temperature.
In Figure 4, a comparison of the obtained mixture fraction contours (in the same experimental window, i.e. 33.71 mm x 14.081 mm from 17.85 mm after injector exit [19]) together with its axial and radial distributions at two axial distances are shown for Test case 1. Clearly, considering that non reacting test conditions are here considered, the mixture fraction has been directly calculated using locally the vapour and air mass fractions. An overall good agreement has been obtained both in terms of axial and radial distributions. Considering the contour plots, vapour concentration seems to be slightly overpredicted mainly in the near axis zone and the difference with experiments tends to decrease going further downstream. This is also confirmed by radial profiles: the jet spreading is underpredicted with a negative impact on the vapour concentration in centerline proximity especially on the first experimental

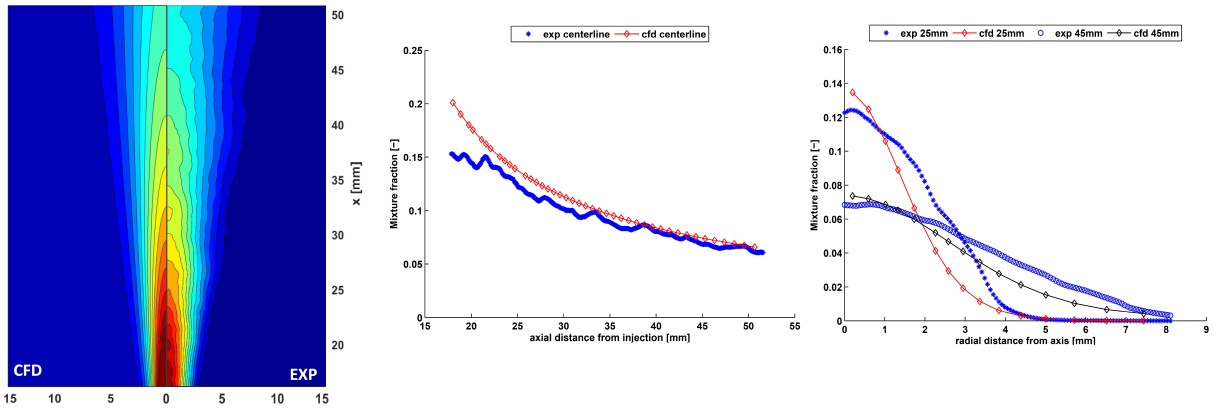

Figure 4. Contours of mixture fraction (left) and axial (center) and radial (right) mixture fraction distributions for Test case 1.

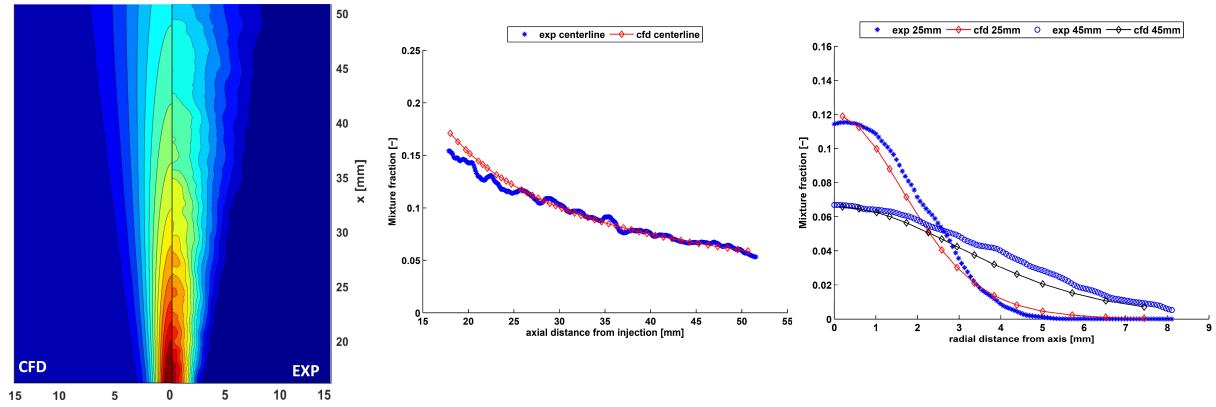

Figure 5. Contour of mixture fraction (left) and axial (center) and radial (right) mixture fraction distributions for Test case 2.

plane. At higher axial distances, the effect of turbulence modelling is less pronounced and numerical results properly reproduce the vapour concentration both in terms of axial and radial distribution. Therefore, based on a physically consistent representation of the gas and turbulence flow-field, the developed code is able to properly predict the local equilibrium state and the final vapour concentration. On the other hand, reducing the axial distance, the effect of turbulence modelling on the solution is more and more important leading, for instance, to an overestimation of mixture fraction at the beginning of the experimental window. Further developments are surely required on this point exploiting scale resolving techniques, such as Large Eddy Simulation, for better catching the liquid/gas interactions. Moreover, the liquid jet penetration was also available on an experimental point of view. Strong attention should be paid on the definition of phase penetration. In technical literature about numerical simulations of the ECN data, several and different definitions on this topic can be found and in the present study, following the work of [20] and [21], the liquid penetration has been evaluated using iso-contour of $\alpha_l = 0.1\%$. In this way it has been possible to evaluate a liquid jet penetration of 10.2 mm which nearly corresponds to the experimental one (i.e. 10.4 mm).
However, to reduce the impact of turbulence modelling and to focus the attention just on evaporation modelling, Test case 2, which is characterized by a lower injection pressure and liquid velocity, has been also considered. Numerical results in terms of mixture fraction contour as well as axial and radial distributions are shown in Figure 5. It should be pointed out that a really good agreement has been obtained for this test case. Thanks to a more physically consistent representation of the flow-field and of the interactions between gas and liquid phase, obtained mixture fraction profiles mimic well the experimental evolution both in terms of axial profile and radial spreading. The pressure and velocity fields together with liquid volume fraction, even in RANS framework, are now correctly reproduced and this leads to properly calculate both the equilibrium state as well as the global evaporation rate.
Finally, it is interesting to point out that on an experimental point of view also the time-dependent penetration of vapour was available for these two test cases. As for the liquid phase, the instantaneous penetration of vapour has been evaluated using the iso-contour of $\alpha_v = 0.1\%$ and obtained results are shown in Figure 6. With a higher injection pressure, the vapour penetration grows faster and this is due to the higher velocity at the exit of the injector. The instantaneous vapour penetration is directly linked to the mass flow rate of the injector but it is also the result of two conflicting phenomena: the increase of velocity makes the liquid penetration growing faster and the turbulence mixing increases the vaporization rate which reduces the liquid penetration. All these phenomena are observed experimentally and recovered by the numerical model. A slight underprediction of penetration can be anyway pointed out mainly considering Test case 2 and it is probably related to a low momentum exchange between vapour and the

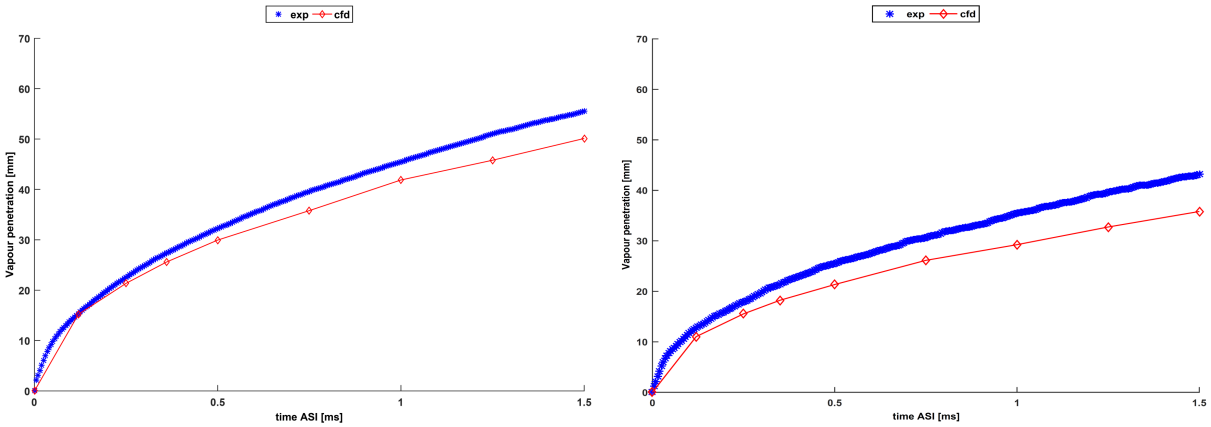

Figure 6. Time-dependent vapour penetrations for Test case 1 (left) and 2 (right).

surrounding air, which can be again related to the performances of the turbulence model. Probably, it is underpredicting the jet spreading and also the interactions between vapour and air at the periphery of the jet, leading to a slower vapour volume fraction mainly concentrated in the near axis region and therefore to a reduced penetration. As already said, scale resolving techniques would help in reducing this gap thanks to a realistic representation of the turbulent flow-field.

Conclusions

This study shows an innovative strategy in modelling spray atomization and in particular in the description of the evaporation in dense spray region where primary break-up takes place. The near injector region is really difficult to characterize experimentally and here the ELSA model has been chosen since it ensures a reliable characterization of the whole atomization process from purely liquid to the dispersed phase. An implicit vaporization model, based on local equilibrium state computation, has been introduced and the entire approach has been successfully tested on an experimental test case representative of diesel injection for two different values of injection pressure. The comparison with experiments shows that the whole approach is able to correctly reproduce the atomization process and to properly catch how evaporation affects the liquid distribution. For both test cases an overall good agreement has been obtained and in particular for Test case 2, where the impact of turbulence modelling should be more reduced, the mixture fraction evolution is well reproduced by numerical computation. In particular, reducing the injection pressure, the model is able to catch the time-dependent reduction of vapour penetration and remaining discrepancies have been justified considering the employed turbulence model. A preliminary validation of the proposed setup is therefore presented and further developments are under investigation for the extension of the whole approach in LES framework.

Nomenclature

Bt	Thermal Spalding number
cp	Specific heat [m^{2}s^{-2}K^{-1}]
D	Laminar Diffusivity [m^{2}s^{-1}]
k	Thermal conductivity [kgms^{-3}K]
m	Mass [kg]
p	Pressure [kgm^{-1}s^{-2}]
Nu	Nusselt number
Sc	Schmidt number
SMD	Sauter Mean Diameter [m]
Pr	Prandtl number
T	Temperature [K]
U	Mixture Velocity [ms^{-1}]

Greek

α_l	Liquid Volume Fraction [-]
Σ	Liquid-gas interface density [m^{-1}]
ρ	Density [kgm^{-3}]
μ	Viscosity [kgm^{-1}s^{-1}]
τ	Evaporation rate [s]

Subscripts

l	Liquid
v	Vapour
a	Air
eq	Equilibrium value
m	Mass
sat	Saturation value
T	Temperature
t	Turbulent quantity

Acronyms

CFD	Computational Fluid Dynamics
$ELSA$	Eulerian Lagrangian Spray Atomization
ECN	European Combustion Network
LES	Large Eddy Simulation
QME	Quasi Multiphase Eulerian

References

[1] ICAO. Enviromental report, aviation and climate change, 2010.

[2] Williams, F. A. Spray combustion and atomization. *Physics of Fluids*, 1(6):541–545, 1958.

[3] F., Laurent and M., Massot. Multi-fluid modelling of laminar polydisperse spray flames: origin, assumptions and comparison of sectional and sampling methods. *Combustion Theory and Modelling*, 5(4):537–572, 2001.

[4] Marchisio, D. L., Pikturna, J. T., Fox, R. O., Vigil, R. D., and Barresi, A. A. Quadrature method of moments for population-balance equations. *AIChE Journal*, 49(5):1266–1276, 2003. ISSN 1547-5905. .

[5] Fox, R.O., Laurent, F., and Massot, M. Numerical simulation of spray coalescence in an eulerian framework: Direct quadrature method of moments and multi-fluid method. *Journal of Computational Physics*, 227(6):3058 – 3088, 2008. ISSN 0021-9991. .

[6] Kah, D., Laurent, F., Massot, M., and Jay, S. A high order moment method simulating evaporation and advection of a polydisperse liquid spray. *Journal of Computational Physics*, 231(2):394 – 422, 2012. ISSN 0021-9991.

[7] F., Michael. Method of moments with interpolative closure. *Chemical Engineering Science*, 57(12):2229 – 2239, 2002. ISSN 0009-2509. Population balance modelling of particulate systems.

[8] Massot, M. *Eulerian Multi-Fluid Models for Polydisperse Evaporating Sprays*, pages 79–123. Springer Vienna, Vienna, 2007. ISBN 978-3-211-72464-4.

[9] Lebas, R., Menard, T., Beau, P.A., Berlemont, A., and Demoulin, F.X. Numerical simulation of primary break-up and atomization: DNS and modelling study. *International Journal of Multiphase Flow*, 35(3):247 – 260, 2009. ISSN 0301-9322.

[10] Vallet, A. and Borghi, R. Modélisation eulerienne de l'atomisation d'un jet liquide. *Comptes Rendus de l'Académie des Sciences - Series IIB - Mechanics-Physics-Astronomy*, 327(10):1015 – 1020, 1999. ISSN 1287-4620.

[11] Andreini, A., Bianchini, C., Puggelli, S., and Demoulin, F.X. Development of a turbulent liquid flux model for eulerian–eulerian multiphase flow simulations. *International Journal of Multiphase Flow*, 81:88 – 103, 2016. ISSN 0301-9322. .

[12] Ning, W., Reitz, R. D., Lippert, A. M., and Diwakar, R. Development of a next-generation spray and atomization model using an eulerian-lagrangian methodology. In *17th International Multidimensional Engine Modeling User's Group Meeting, Detroit, MI, April 2007*, 2007.

[13] Kösters, A. and Karlsson, A. A comprehensive numerical study of diesel fuel spray formation with openfoam. Technical report, SAE Technical Paper, 2011.

[14] Garcia-Oliver, J. M, Pastor, J. M, Pandal, A., Trask, N., Baldwin, E., and Schmidt, D. P. Diesel spray cfd simulations based on the σ-y eulerian atomization model. *Atomization and Sprays*, 23(1), 2013.

[15] Desantes, J. M., Garcia-Oliver, J. M., Pastor, J. M., and Pandal, A. A comparison of diesel sprays cfd modeling approaches: Ddm versus σ-y eulerian atomization model. *Atomization and Sprays*, 26(7):713–737, 2016. ISSN 1044-5110.

[16] Chrigui, M., Gounder, J., Sadiki, A., Masri, A. R., and Janicka, J. Partially premixed reacting acetone spray using LES and FGM tabulated chemistry. *Combustion and Flame*, 159(8):2718 – 2741, 2012. ISSN 0010-2180. Special Issue on Turbulent Combustion.

[17] Abramzon, B. and Sirignano, W.A. Droplet vaporization model for spray combustion calculations. *International Journal of Heat and Mass Transfer*, 32(9):1605 – 1618, 1989. ISSN 0017-9310.

[18] Chin, J.S. and Lefebvre, A.H. The Role of the Heat-up Period in Fuel Drop Evaporation. *International Journal of Turbo and Jet Engines*, 1985. .

[19] ECN. Engine combustion network, 2012. URL `https://ecn.sandia.gov/`.

[20] Khuong, A. D. *The Eulerian-Lagrangian Spray Atomization (ELSA) model of the jet atomization in CFD simulations: evaluation and validation*. PhD thesis, Universitat Politécnica de Valéncia, 2012.

[21] Kralj, C. *Numerical simulation of Diesel spray processes*. PhD thesis, University of London, 1996.